# A Bayesian approach to SENSE Image Reconstruction in FMRI

Daniel B. Rowe[1,2]
[1]Department of Mathematics, Statistics and Computer Science, Marquette University
[2]Department of Biophysics, Medical College of Wisconsin

## Abstract

In fMRI, it is important to acquire volume images of the brain as rapidly as possible to capture cognitive temporal dynamics. The limiting temporal factor in fMRI is the sampling time for an array of spatial frequencies to reconstruct an image. The multi-coil SENSE in-plane reconstruction technique has greatly contributed to decreasing image scan time. However, the SENSE image reconstruction technique involves using *a priori* calibration images to estimate coil sensitivities, then using these estimated coil sensitivities as if they were precisely known to reconstruct images. Here, the *a priori* calibration image information is quantified in terms of a prior distribution on the reconstructed image and coil sensitivities, then combined with the data likelihood in order to form a posterior distribution that the reconstructed image is estimated from. This Bayesian SENSE (BSENSE) formally brings the prior image information to bear while estimating the reconstructed image in one step from the posterior distribution. BSENSE is applied to simulated data.

**Key Words:** fMRI, Bayesian, SENSE, reconstruction

## 1. Introduction

### 1.1 Background

In the early 1990's, fMRI (functional magnetic resonance imaging) was developed as a technique to noninvasively observe the human brain in action (1). FMRI is based upon the BOLD (blood oxygen level dependent contrast) in which blood oxygenation changes in the local vicinity of firing neurons (2). In fMRI and MRI, voxel values are not measured by the machine, the measurements taken by the machine are an array of complex-valued spatial frequencies called *k*-space (3). It generally takes up to two seconds to measure full arrays of data for all of the slices that form the volume image. A tremendous amount of work has been and is currently being devoted to accelerating the number of images acquired per unit of time since its initial postulation (4). Significant advances in accelerating image acquisition have been made by utilizing multiple local coils and subsampling *k*-space in an image plane by skipping lines in-plane. When lines of *k*-space are skipped, the reconstructed coil images are aliased. Two major approaches have been developed to unalias in-plane aliased images due to skipped lines of *k*-space. The first, SENSitivity Encoding (SENSE) operates on aliased images after reconstruction (5), while the second GeneRalized Autocalibrating Partial Parallel Acquisition (GRAPPA) operates on subsampled *k*-space prior to reconstruction (6). The technique described here is a Bayesian version of the SENSE image space approach (BSENSE). In order to lead up to the current work, single-coil full *k*-space inverse Fourier transform (IFT) image reconstruction needs to first be described, then multi-coil full-sampled *k*-space IFT image reconstruction with SENSE image combination, and finally multi-coil sub-sampled *k*-space with SENSE image combination. The entirety of what is discussed here will be for Cartesian *k*-space.

### 1.2 Single-Coil Full-Sampled *k*-Space Image Reconstruction

Historically, a single channel coil as depicted in Figure 1 (left) was utilized for fMRI to measure a full-sampled *k*-space data array of the same dimensions as the image to be reconstructed as depicted in Figure 1 (right). In Figure 1 (right), *k*-space data is measured in a zig-zag fashion from left to right and bottom to top.

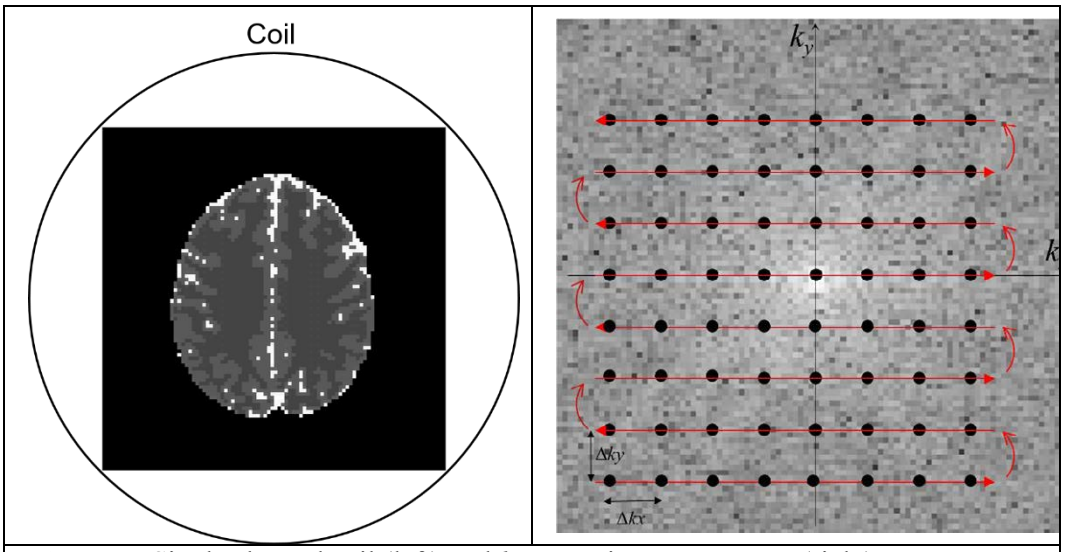


**Figure 1:** Single channel coil (left) and *k*-space zig-zag coverage (right).

Measured *k*-space data is truly complex-valued as displayed in Figure 2 (column 2) with a real part (top) and imaginary part (bottom). This complex-valued *k*-space data is reconstructed by pre-multiplying with a complex-valued inverse Fourier transform matrix in Figure 2 (column 1) with a real part (top) and imaginary part (bottom) then post-multiplying by the transpose of an inverse Fourier transform matrix in Figure 2 (column 3) with a real part (top) and imaginary part (bottom). The result of this complex-valued pre- and post-multiplication by inverse Fourier transform matrices is a complex-valued reconstructed image (column 4) with real part (top) and imaginary part (bottom).

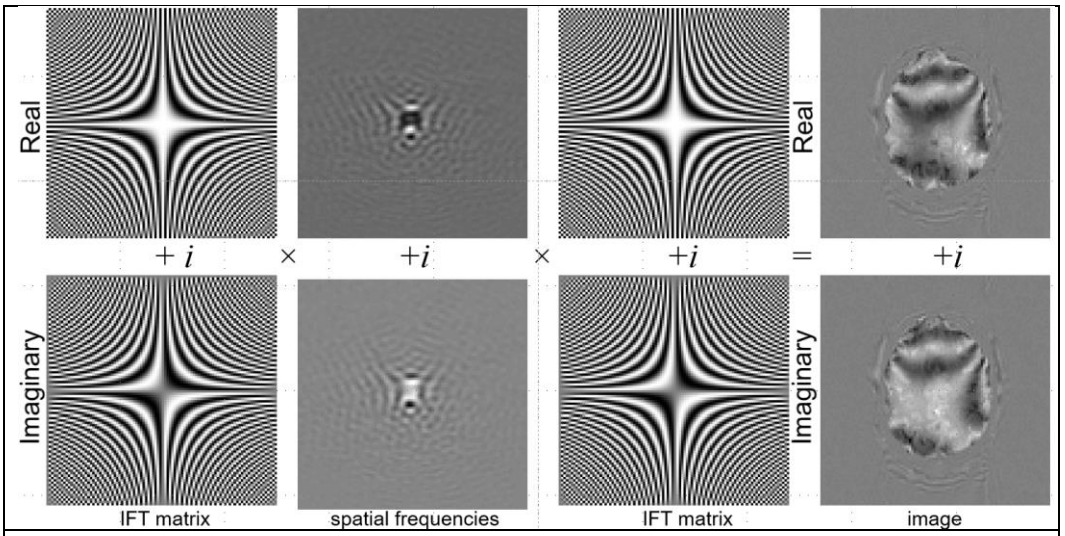


**Figure 2:** Inverse Fourier transform image reconstruction of a complex-valued *k*-space array to a complex-valued image.

Since the magnitude (and phase) of a reconstructed image is generally utilized for fMRI analysis, Figure 3 is a duplicate of Figure 2 except the fourth column displays magnitude (top) and phase (bottom) instead of real and imaginary. This is a conversion from Cartesian coordinates to polar coordinates.

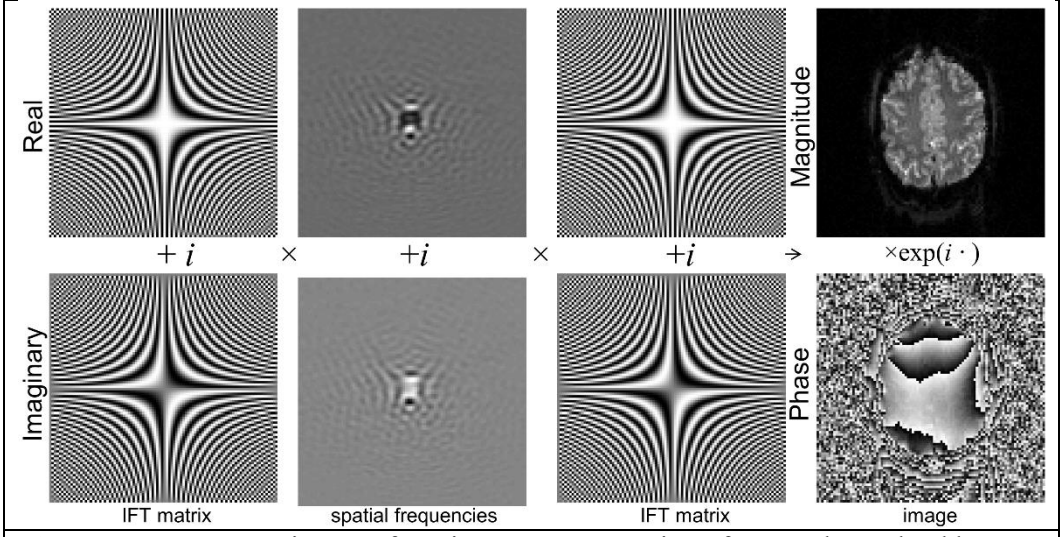


**Figure 3:** Inverse Fourier transform image reconstruction of a complex-valued k-space array to a magnitude and phase image.

A series of these reconstructed images is produced while the subject is performing a task and either the magnitude alone can be utilized for activation (1) or both the magnitude and phase (8,9).

### 1.3 Multi-Coil Full-Sampled *k*-Space Image Reconstruction

In recent years, multi coil arrays have been used to acquire data to produce slice images. Instead of a single channel coil as in Figure 1 (left), multiple local coils such as the illustrative example in Figure 4 (left) with $N_C$=4 coils are used. In Figure 4 (left), coil 1 is on the top, coil 2 on the right, coil 3 on the bottom, and coil 4 on the left. To begin with in this subsection, each coil can measure a full-sampled *k*-space array as depicted in Figure 4 (right), and later in the next subsection each coil will measure a sub-sampled *k*-space array by skipping lines.

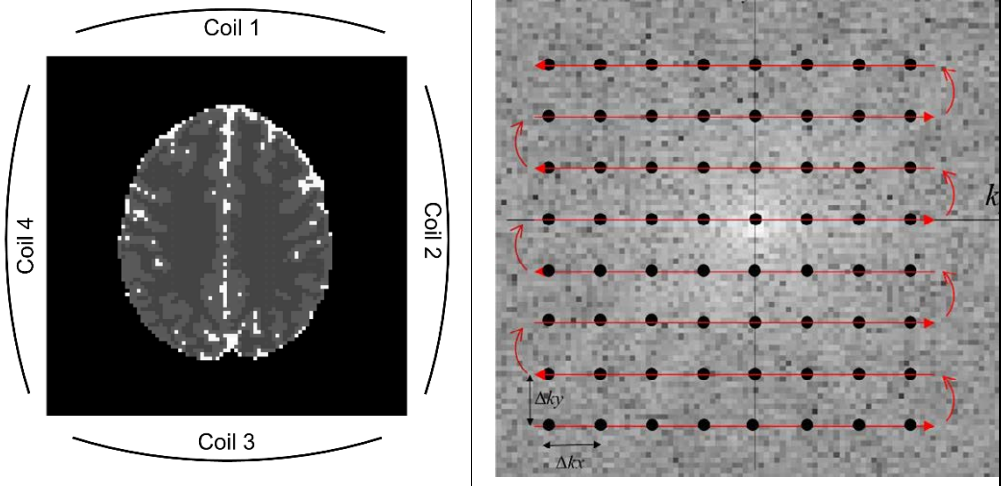


**Figure 4:** Four channel coil (left) and *k*-space zig-zag coverage (right).

Each local receive coil, possesses a depth sensitivity profile that is related to its size measuring a different sensitivity weighted version of the true slice. Subfigures in Figure 5 and subsequent figures will have rows referred as top, middle, bottom and columns referred to as left, center, and right. In Figure 5 (middle center) is a true slice image with a particular voxel $v$ indicated with a red circle. The depth sensitivity profile for coil 1 is given in Figure 5 (top) with sensitivity $S_1$ for voxel $v$. Neglecting noise, coil 1 measures a *k*-space array that after inverse Fourier transform reconstruction is the true image point-wise multiplied by the sensitivity profile for coil 1, $a_1=S_1v$ as in Figure 5 (top right). Similarly without noise, coil 2 measures a *k*-space array that after inverse Fourier transform reconstruction is the true image point-wise multiplied by the sensitivity profile for coil 2, $a_2=S_2v$ as in Figure 5 (center right), coil 3 measures a *k*-space array that after inverse Fourier transform reconstruction is the true image point-wise multiplied by the sensitivity profile for coil 3, $a_3=S_3v$ as in Figure 5 (bottom left), coil 4 measures a *k*-space array that after inverse Fourier transform reconstruction is the true image point-wise multiplied by the sensitivity profile for coil 4, $a_4=S_4v$ as in Figure 5 (top left).

With these $N_C=4$ coil measurements, a system of equations can be formed as in Equation 1 where $a=[a_1,a_2,a_3,a_4]'$ are the observed coil measurements, $S=[S_1,S_2,S_3,S_4]'$ are the unobserved coil sensitivities, and $v$ is the unobserved true slice voxel value.

$$\begin{bmatrix} a_1 \\ a_2 \\ a_3 \\ a_4 \end{bmatrix} = \begin{bmatrix} S_1 \\ S_2 \\ S_3 \\ S_4 \end{bmatrix} v \qquad [1]$$

If we are able to obtain an estimate of the coil sensitivities $\hat{S}$, then we can obtain a least squares estimate of the true slice voxel value $v$ as

$$\hat{v} = (\hat{S}'\hat{S})^{-1}\hat{S}'a \ . \qquad [2]$$

This is repeated individually for each voxel in the image.

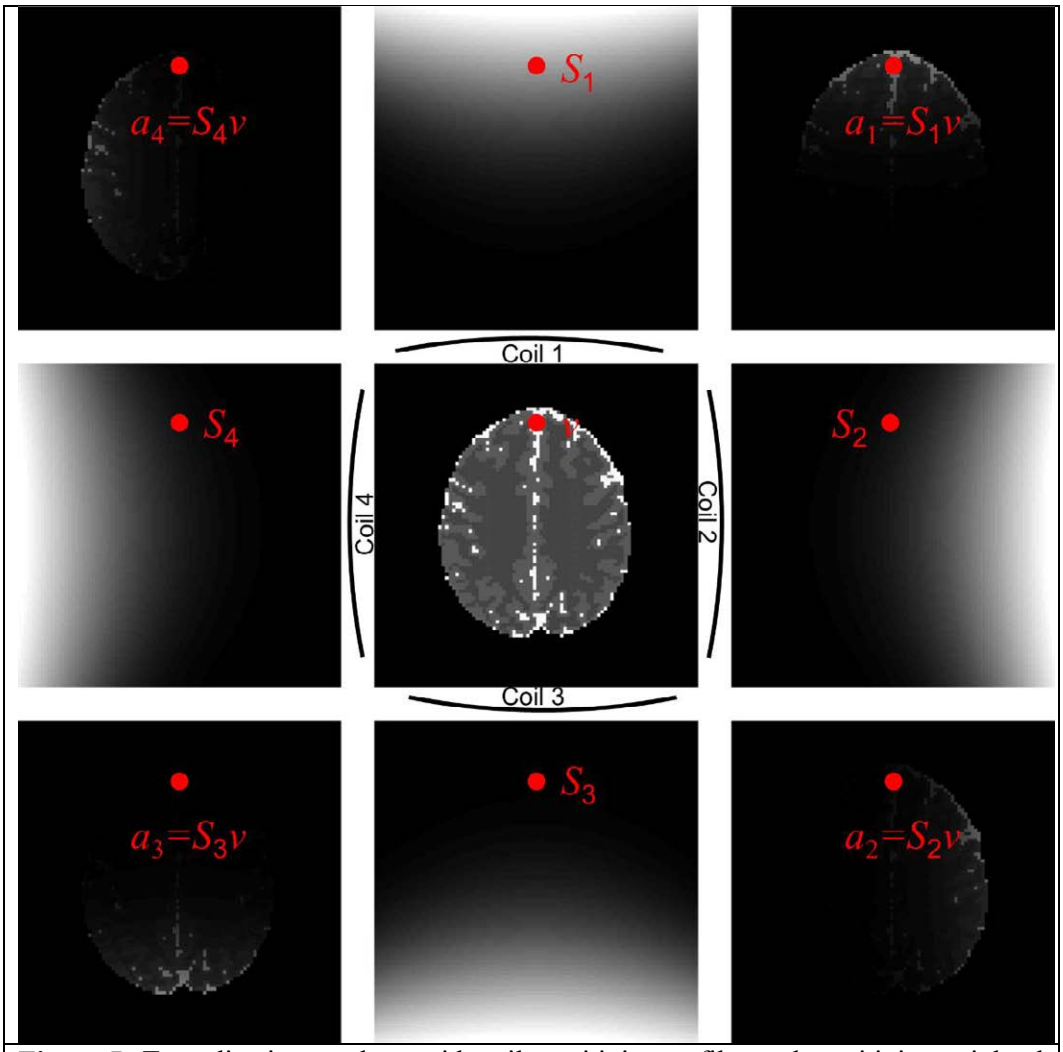


**Figure 5:** True slice image along with coil sensitivity profiles and sensitivity weighted true images.

However, the goal is to obtain slice images faster. It takes an appreciable amount of time to measure a complex-valued *k*-space data array. For example, for a 96×96 image and the equivalent of approximately 83 elements in each turn-around for 95 turn-arounds totaling 96×96+95×83=772,813 complex-valued points for the *k*-space array along with some additional time spent with other items such as slice selection and wait time for the gradient echo to bring the total time for about 7 to 11 slices close to a 1 s time to repetition (TR).

### 1.4 Multi-Coil Sub-Sampled *k*-Space Image Reconstruction

As previously noted, the goal is to accelerate the number of images acquired per unit time. Because there are limitations on how fast we can traverse *k*-space and measureits' *k*-space data values, it is of great interest to develop ways to measure less data, but still be able to form an image. As previously noted, one way that this is accomplished is to skip lines of *k*-space and not measure the corresponding array data values. Figure 6 (right) contains an illustration of skipping lines of *k*-space in the vertical direction and measuring every third line with measured black circle data values and not measuring intermediate white circled data values. Measuring every third line results in an acceleration factor $A$=3.

The consequence of inverse Fourier transform reconstruction of the rectangular coil *k*-space arrays is that the reconstructed image has aliasing in the direction of the skipped lines. With an acceleration factor of $A$=3, the reconstructed coil images will appear as if the full image had been cut into three equal horizontal strips and the strips summed.

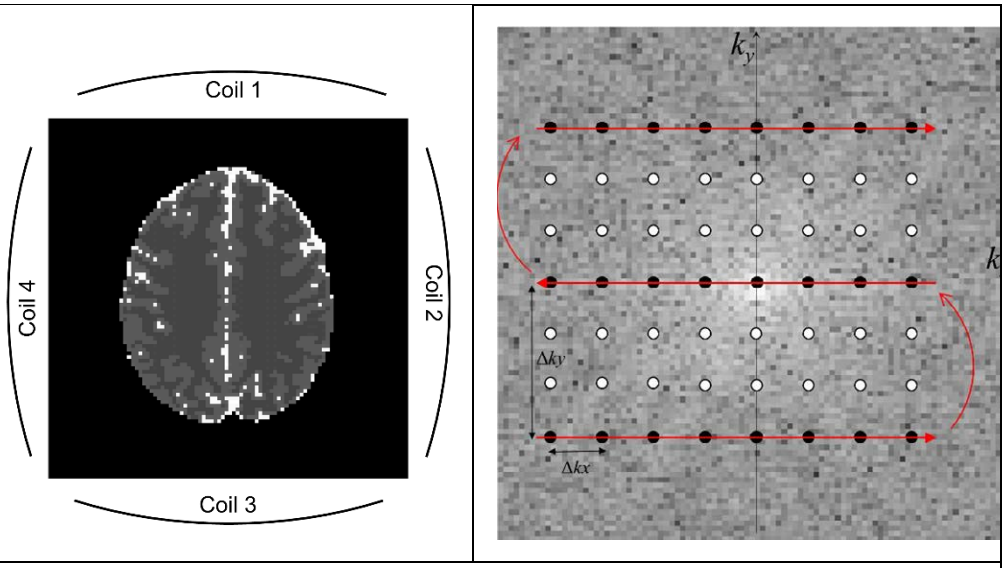


**Figure 6:** Four channel coil (left) and *k*-space zig-zag coverage (right).

Each coil measures a different sensitivity weighted version of the true slice. In Figure 7 (middle center) is a true slice image with $A$=3 voxels $v_1$, $v_2$, $v_3$ in a particular column and same row in each strip indicated with red, green, and blue circles. The depth sensitivity profile for coil 1 is given in Figure 7 (top) with sensitivity $S_{11}$ for voxel $v_1$, sensitivity $S_{12}$ for voxel $v_2$, sensitivity $S_{13}$ for voxel $v_3$.

Neglecting noise, coil 1 measures a rectangular *k*-space array that after inverse Fourier transform reconstruction produces an aliased rectangular image that is the sum of three horizontal strips of the full true image as in Figure 7 (top right). In Figure 7 (top right) the true aliased image is the point-wise multiplication of the given voxel by the sensitivity profile for coil 1 summed for the three strips, $a_1=S_{11}v_1+S_{12}v_2+S_{13}v_3$. Similarly without noise, coil 2 measures a rectangular *k*-space array that after inverse Fourier transform reconstruction is the point-wise multiplication of the given voxel by the sensitivity profile for coil 2 summed for the three strips, $a_2=S_{21}v_1+S_{22}v_2+S_{23}v_3$ as in Figure 7 (bottom right), coil 3 measures a rectangular *k*-space array that after inverse Fourier transform reconstruction is the point-wise multiplication of the given voxel by the sensitivity profile for coil 3 summed for the three strips, $a_3=S_{31}v_1+S_{32}v_2+S_{33}v_3$ as in Figure 7 (bottom left), coil 4 measures a rectangular *k*-space array that after inverse Fourier transform reconstruction is the point-wise multiplication of the given voxel by the sensitivity profile for coil 4 summed for the three strips, $a_4=S_{41}v_1+S_{42}v_2+S_{43}v_3$ as in Figure 7 (top left).

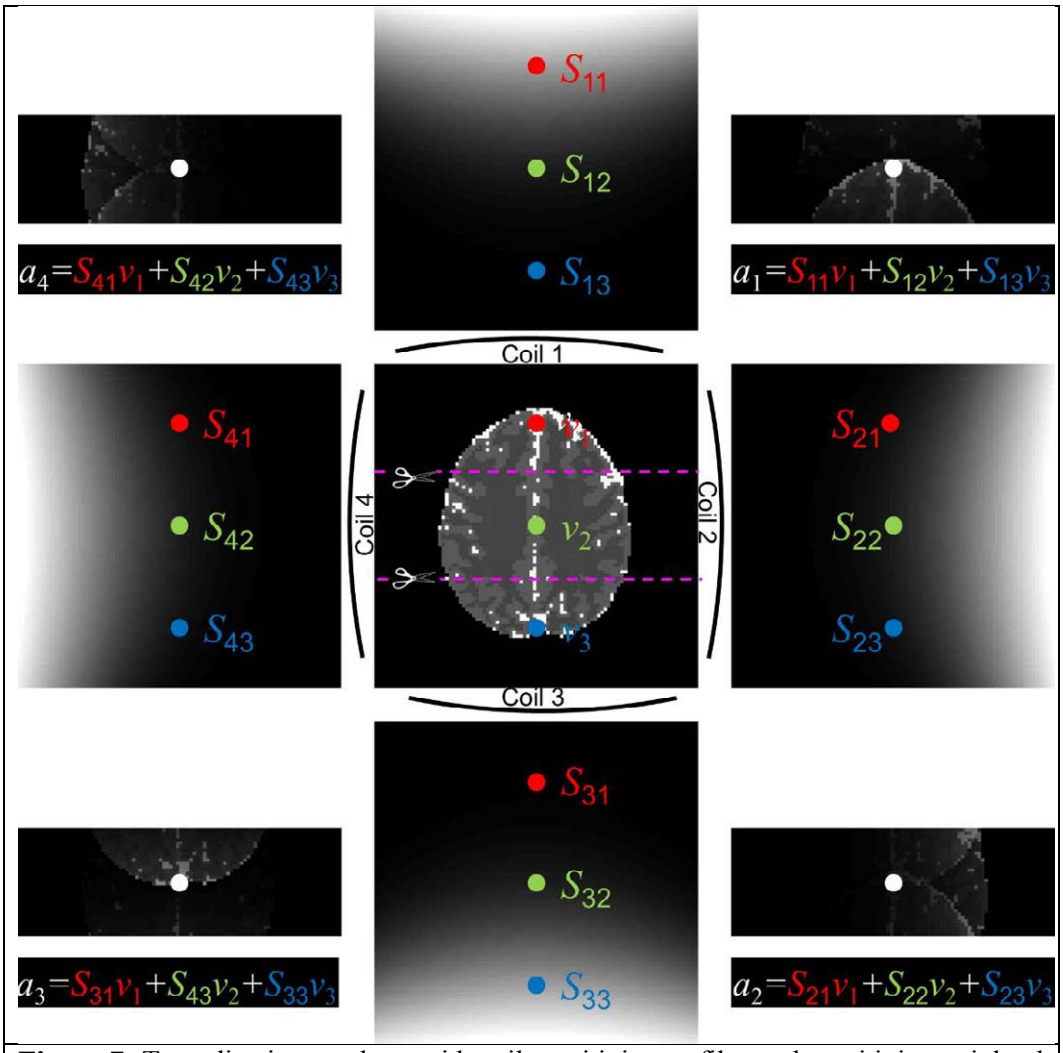


**Figure 7:** True slice image along with coil sensitivity profiles and sensitivity weighted true aliased images.

With these $N_C$=4 coil measurements, a system of equations can be formed similar to Equation 1 where $a=[a_1,a_2,a_3,a_4]'$ are the observed coil measurements, $S=[[S_{11},S_{21},S_{31},S_{41}]',[S_{12},S_{22},S_{32},S_{42}]',[S_{13},S_{23},S_{33},S_{43}]']$ are the unobserved coil sensitivities, and $v=[v_1,v_2,v_3]'$ is the unobserved true slice voxel values.

$$\begin{bmatrix} a_1 \\ a_2 \\ a_3 \\ a_4 \end{bmatrix} = \begin{bmatrix} S_{11} & S_{12} & S_{13} \\ S_{21} & S_{22} & S_{23} \\ S_{31} & S_{32} & S_{33} \\ S_{41} & S_{42} & S_{43} \end{bmatrix} \begin{bmatrix} v_1 \\ v_2 \\ v_3 \end{bmatrix} \qquad [3]$$

In Equation 3, $a$ is $N_C\times1$, $S$ is $N_C\times A$, and $v$ is $A\times1$. If we are able to obtain an estimate of the coil sensitivities $\hat{S}$, then we can obtain a least squares estimate of the $A$ true slice voxel values $v$ as

$$\hat{v} = (\hat{S}'\hat{S})^{-1}\hat{S}'a \quad . \qquad [4]$$

This is repeated individually for each voxel in the aliased image. In addition, $\hat{S}'\hat{S}$ is not in general positive definite.

## 2. Bayesian Multi-Coil Sub-Sampled *k*-Space Image Reconstruction

### 2.1 The Complex-Valued Nature of SENSE Image Reconstruction

The figures in the previous section were all illustrative. In actuality, the entire problem is complex-valued. Given the existence of $N_C$=4 receive coils as in Figures 4 and 6 (left), each local receive coil possesses a depth sensitivity profile that is related to its size, but the sensitivity is complex-valued. Each coil measures a different complex-valued sensitivity weighted version of the true complex-valued slice. In Figure 8 (middle center) is a true complex-valued slice image with a particular voxel $v=v_R+iv_I$ indicated with red circles. The complex-valued depth sensitivity profile for coil 1 is given in Figure 8 (top) with sensitivity $S_1=S_{1R}+S_{1I}$ for voxel $v=v_R+iv_I$. Neglecting noise, coil 1 measures a *k*-space array that after inverse Fourier transform reconstruction is the true complex-valued image point-wise multiplied by the complex-valued sensitivity profile for coil 1, $a_{1R}+a_{1I}=(S_{1R}+iS_{1I})(v_R+iv_I)$ or $a_1=S_1v$ as in Figure 8 (top right). Similarly without noise, coil 2 measures a *k*-space array that after inverse Fourier transform reconstruction is the true complex-valued image point-wise multiplied by the complex-valued sensitivity profile for coil 2, $a_{2R}+a_{2I}=(S_{2R}+iS_{2I})(v_R+iv_I)$ or $a_2=S_2v$ as in Figure 8 (center right), coil 3 measures a *k*-space array that after inverse Fourier transform reconstruction is the true image point-wise multiplied by the sensitivity profile for coil 3, $a_{3R}+a_{3I}=(S_{3R}+iS_{3I})(v_R+iv_I)$ or $a_3=S_3v$ as in Figure 8 (bottom left), coil 4 measures a *k*-space array that after inverse Fourier transform reconstruction is the true image point-wise multiplied by the sensitivity profile for coil 4, $a_{4R}+a_{4I}=(S_{4R}+iS_{4I})(v_R+iv_I)$ or $a_4=S_4v$ as in Figure 8 (top left).

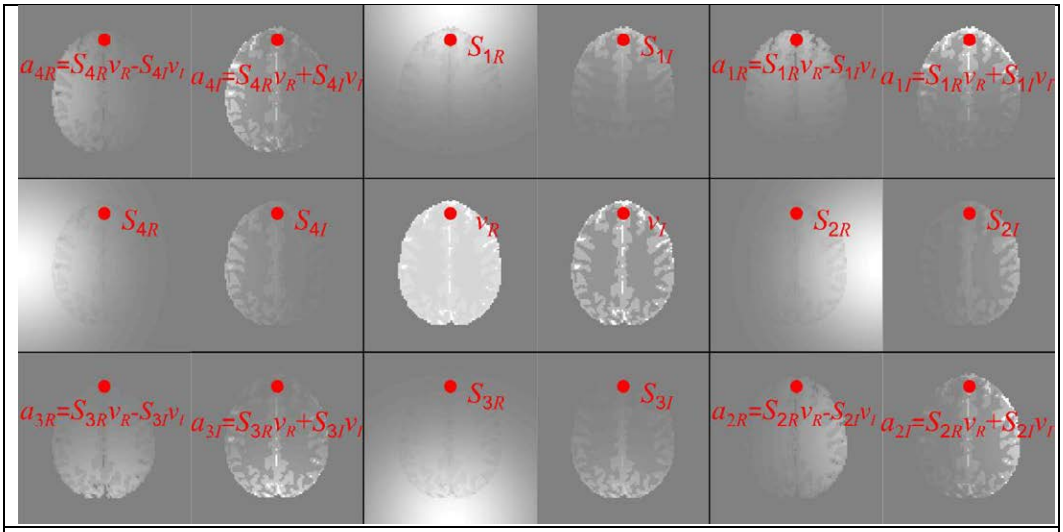


**Figure 8:** True slice complex-valued image along with complex-valued coil sensitivity profiles and complex-valued sensitivity weighted true images.

With these $N_C$=4 coil measurements, a system of equations can be formed in Equation 5 similar to Equation 1 except now all quantities are complex-valued. In Equation 5, the *a*'s are observed while the *S*'s and *v*'s are unobserved.

$$\begin{bmatrix} a_{1R}+ia_{1I} \\ a_{2R}+ia_{2I} \\ a_{3R}+ia_{3I} \\ a_{4R}+ia_{4I} \end{bmatrix} = \begin{bmatrix} S_{1R}+iS_{1I} \\ S_{2R}+iS_{2I} \\ S_{3R}+iS_{3I} \\ S_{4R}+iS_{4I} \end{bmatrix} \begin{bmatrix} v_R+iv_I \end{bmatrix} \quad [5]$$

It can be shown that an equivalent representation of Equation 5 is

$$\begin{bmatrix} a_{1R} \\ a_{2R} \\ a_{3R} \\ a_{4R} \\ a_{1I} \\ a_{2I} \\ a_{3I} \\ a_{4I} \end{bmatrix} = \begin{bmatrix} S_{1R} & -S_{1I} \\ S_{2R} & -S_{2I} \\ S_{3R} & -S_{3I} \\ S_{4R} & -S_{4I} \\ S_{1I} & S_{1R} \\ S_{2I} & S_{2R} \\ S_{3I} & S_{3R} \\ S_{4I} & S_{4R} \end{bmatrix} \begin{bmatrix} v_R \\ v_I \end{bmatrix} \quad [6]$$

Or more compactly as $a=Sv$ where $a$ is $2N_C\times1$, $S$ is $2N_C\times2$, and $v$ is $2\times1$. If we are able to obtain an estimate of the coil sensitivities $\hat{S}$, then we can obtain a least squares estimate of the true slice voxel value $v$ as

$$\hat{v} = (\hat{S}'\hat{S})^{-1}\hat{S}'a \quad . \quad [7]$$

This is repeated individually for each voxel in the image. In addition, $\hat{S}'\hat{S}$ is not in general positive definite.

However, because we want to accelerate the number of slices acquired per unit of time, we again skip lines of *k*-space for each coil as illustrated in Figure 6. Neglecting noise, coil 1 measures a rectangular *k*-space array that after inverse Fourier transform reconstruction produces an aliased rectangular image that is the sum of three horizontal strips of the full true image as in Figure 9 (top right). In Figure 9 (top right) the true complex-valued aliased image is the point-wise multiplication of the given complex-valued voxel by the complex-valued sensitivity profile for coil 1 summed for the three strips, $a_{1R}=S_{11R}v_{1R}+S_{12R}v_{2R}+S_{13R}v_{3R}-S_{11I}v_{1I}-S_{12I}v_{2I}-S_{13I}v_{3I}$ and $a_{1I}=S_{11I}v_{1R}+S_{12I}v_{2R}+S_{13I}v_{3R}+S_{11R}v_{1I}+S_{12R}v_{2I}+S_{13R}v_{3I}$. Similarly without noise, coil 2 measures a rectangular *k*-space array that after inverse Fourier transform reconstruction is the point-wise multiplication of the given complex-valued voxel by the complex-valued sensitivity profile for coil 2 summed for the three strips, $a_{2R}=S_{21R}v_{1R}+S_{22R}v_{2R}+S_{23R}v_{3R}-S_{21I}v_{1I}-S_{22I}v_{2I}-S_{23I}v_{3I}$ and $a_{2I}=S_{21I}v_{1R}+S_{22I}v_{2R}+S_{23I}v_{3R}+S_{21R}v_{1I}+S_{22R}v_{2I}+S_{23R}v_{3I}$ as in Figure 9 (bottom right), coil 3 measures a rectangular *k*-space array that after inverse Fourier transform reconstruction is the point-wise multiplication of the given complex-valued voxel by the complex-valued sensitivity profile for coil 3 summed for the three strips, $a_{3R}=S_{31R}v_{1R}+S_{32R}v_{2R}+S_{33R}v_{3R}-S_{31I}v_{1I}-S_{32I}v_{2I}-S_{33I}v_{3I}$ and $a_{3I}=S_{31I}v_{1R}+S_{32I}v_{2R}+S_{33I}v_{3R}+S_{31R}v_{1I}+S_{32R}v_{2I}+S_{33R}v_{3I}$ as in Figure 9 (bottom left), coil 4 measures a rectangular *k*-space array that after inverse Fourier transform reconstruction is the point-wise multiplication of the given complex-valued voxel by the complex-valued sensitivity profile for coil 4 summed for the three strips, $a_{4R}=S_{41R}v_{1R}+S_{42R}v_{2R}+S_{43R}v_{3R}-S_{41I}v_{1I}-S_{42I}v_{2I}-S_{43I}v_{3I}$ and $a_{4I}=S_{41I}v_{1R}+S_{42I}v_{2R}+S_{43I}v_{3R}+S_{41R}v_{1I}+S_{42R}v_{2I}+S_{43R}v_{3I}$ as in Figure 9 (top left).

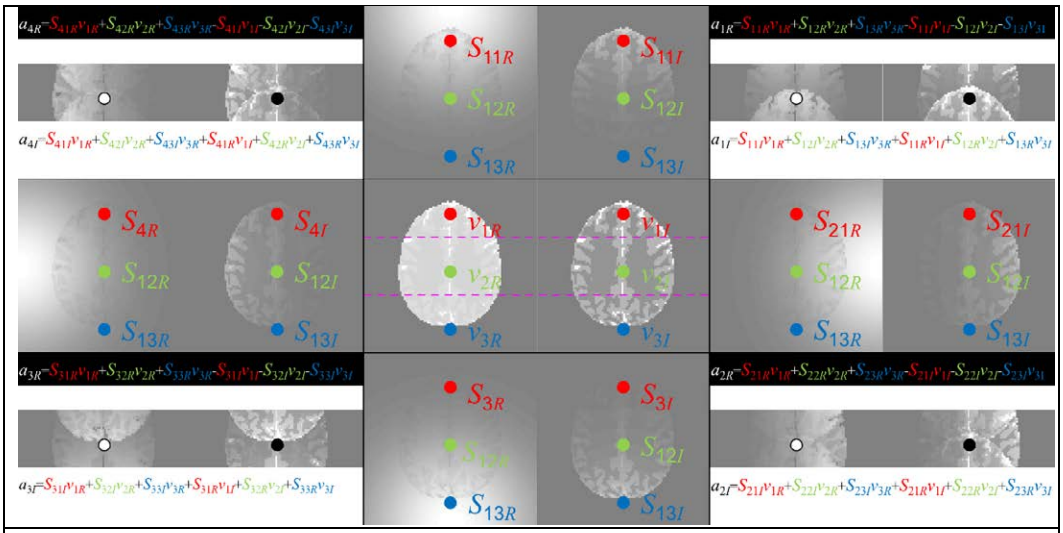

**Figure 9:** True slice image along with coil sensitivity profiles and sensitivity weighted true aliased images.

With these $N_C$=4 coil measurements, a system of equations can be formed as in Equation 8 where $a=[a_{1R},a_{2R},a_{3R},a_{4R},a_{1I},a_{2I},a_{3I},a_{4I}]'$ are the observed coil measurements, $S$ as defined below are the unobserved coil sensitivities, and $v=[v_{1R},v_{2R},v_{3R},v_{1I},v_{2I},v_{3I}]'$ is the unobserved true slice voxel values.

$$\begin{bmatrix} a_{1R} \\ a_{2R} \\ a_{3R} \\ a_{4R} \\ a_{1I} \\ a_{2I} \\ a_{3I} \\ a_{4I} \end{bmatrix} = \begin{bmatrix} S_{11R} & S_{12R} & S_{13R} & -S_{11I} & -S_{12I} & -S_{13I} \\ S_{21R} & S_{22R} & S_{23R} & -S_{21I} & -S_{22I} & -S_{23I} \\ S_{31R} & S_{32R} & S_{33R} & -S_{31I} & -S_{32I} & -S_{33I} \\ S_{41R} & S_{42R} & S_{43R} & -S_{41I} & -S_{42I} & -S_{43I} \\ S_{11I} & S_{12I} & S_{13I} & S_{11R} & S_{12R} & S_{13R} \\ S_{21I} & S_{22I} & S_{23I} & S_{21R} & S_{22R} & S_{23R} \\ S_{31I} & S_{32I} & S_{33I} & S_{31R} & S_{32R} & S_{33R} \\ S_{41I} & S_{42I} & S_{43I} & S_{41R} & S_{42R} & S_{43R} \end{bmatrix} \begin{bmatrix} v_{1R} \\ v_{2R} \\ v_{3R} \\ v_{1I} \\ v_{2I} \\ v_{3I} \end{bmatrix} \quad [8]$$

Or more compactly as $a=Sv$ where $a$ is $2N_C\times1$, $S$ is $2N_C\times2A$, and $v$ is $2A\times1$. If we are able to obtain an estimate of the coil sensitivities $\hat{S}$, then we can obtain a least squares estimate of the true slice voxel values $v$ as

$$\hat{v} = (\hat{S}'\hat{S})^{-1}\hat{S}'a \quad . \quad [9]$$

This is repeated individually for each voxel in the aliased image. In addition, $\hat{S}'\hat{S}$ is not in general positive definite. Equation 8 is a latent variable model similar to factor analysis but complex-valued (12).

## 2.2 Distributions and Estimation

### 2.2.1 Likelihood Distribution

In an fMRI experiment as described for Equation 8, the aliased voxel measurements are taken with measurement error so $a=Sv+\varepsilon$ where $a$ is $2N_C\times1$, $S$ is $2N_C\times2A$, $v$ is $2A\times1$, and $\varepsilon$ is $2A\times1$. It is assumed that $\varepsilon \sim N(0,\sigma^2 I)$. The likelihood for the measurements is

$$p(a \mid S, v, \sigma^2) \propto (\sigma^2)^{-\frac{2N_C}{2}} \exp\left[ -\frac{1}{2\sigma^2}(a - Sv)'(a - Sv) \right] \quad [10]$$

where $a$ observed aliased, $S$ unobserved sensitivities, and $v$ unobserved voxel values.

### 2.2.2 Prior Distributions

From the likelihood distribution, it can be seen that prior distributions need to be specified for $(S,v,\sigma^2)$ and hyperparameters assessed. For the coil sensitivities $S$ and the voxel values $v$, normally distributed $g$-priors are specified and for the noise variance $\sigma^2$ an inverse gamma distribution is specified. Together, these prior distributions are

$$\begin{aligned} p(S \mid \sigma^2) &\propto (\sigma^2)^{-\frac{2N_C A}{2}} \exp\left[ -\frac{g_S}{2\sigma^2} tr(S - S_0)'(S - S_0) \right] \\ p(v \mid \sigma^2) &\propto (\sigma^2)^{-\frac{2N_C A}{2}} \exp\left[ -\frac{g_v}{2\sigma^2}(v - v_0)'(v - v_0) \right] \\ p(\sigma^2) &\propto (\sigma^2)^{-\frac{d}{2}-1} \exp\left[ -\frac{q}{2\sigma^2} \right] \end{aligned} \quad [11]$$

with hyperparameters $g_S$, $S_0$, $g_v$, $v_0$, $d$, and $q$ to be assessed.

### 2.2.3 Posterior Distribution

With the combination of the priors and the likelihood, the posterior distribution for the coil sensitivities $S$, the voxel values $v$, and for the noise variance $\sigma^2$ the posterior distribution is

$$p(S, v, \sigma^2 \mid a) \propto p(S \mid \sigma^2) p(v \mid \sigma^2) p(\sigma^2) p(a \mid S, v, \sigma^2) \quad [12]$$

with distributions specifically described above in Equations 11 and 12.

### 2.2.4 MAP Estimation

From the posterior distribution in Equation 12 with priors detailed in Equation 11 and likelihood in Equation 10, the modes for the parameters to be estimated are

$$\begin{aligned} \hat{S} &= (g_S S_0 + av')(g_S I + v'v)^{-1} \\ \hat{v} &= (g_v I + S'S)^{-1}(g_v v_0 + S'a) \\ \hat{\sigma}^2 &= [(a - Sv)'(a - Sv) + g_v(v - v_0)'(v - v_0) + dq \\ &\quad + g_S tr(S - S_0)(S - S_0)] / [2(2N_C + 2A + d + 2N_C A + 1)] \end{aligned} \quad . \quad [13]$$

Maximum a posteriori (MAP) estimates of the parameters will be found using the ICM algorithm (11). Alternatively a Gibbs sampler can be utilized to obtain posterior means (12).

## 3. Results

### 3.1 Hyperparameter Assessment

Prior to an fMRI experiment, a short non-task based set of $m$ full $k$-space volume images for the $N_C$ coils can be obtained similar to Figure 8. These "calibration" images can be utilized to assess the hyperparameters of the prior distributions for the parameters. These $m$ calibration images can be averaged as in Figure 10.

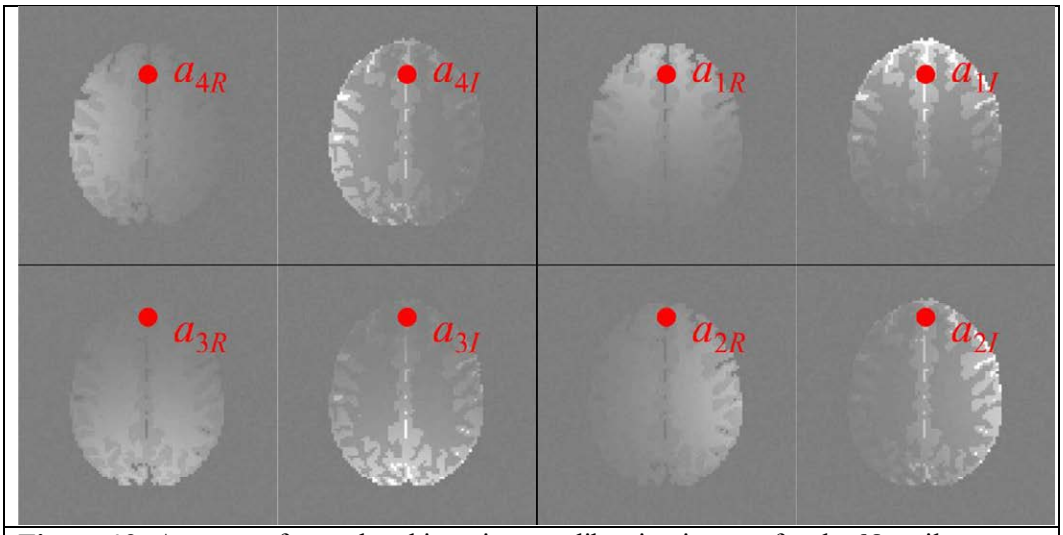


**Figure 10:** Average of $m$ real and imaginary calibration images for the $N_C$ coils.

The root sum of squares in each voxel is computed from these $N_C$=4 complex-valued coil images

$$v_{0M} = \left[ a_{R1}^2 + a_{1I}^2 + a_{2R}^2 + a_{2I}^2 + a_{3R}^2 + a_{3I}^2 + a_{4R}^2 + a_{4I}^2 \right]^{1/2} \qquad [14]$$

for the an initial magnitude $v_{0M}$ of the prior mean as in Equations 14. However there has to be an adjustment made at the center of the image due to nonuniform coil coverage. The initial prior mean magnitude in Figure 11 (left) is pointwise multiplied (Hadamard product, $\odot$) by a Gaussian hill

$$h(x,y) = 1.1 + .4 \times \exp\left\{ -\frac{1}{2n_{xy}} \left[ (x - n_{xy}/2 - 1)^2 + (-n_{xy}/2 - 1)^2 \right] \right\} \qquad [15]$$

as in Figure 11 (middle) to account for this nonuniformity as in Figure 11 (right) for a revised $v_{0M}$. The hyper parameter $g_v$ is assessed to be 0.10 to indicate that the uncertainty in the prior voxel values is ten times larger than that in the observed aliased coil images.

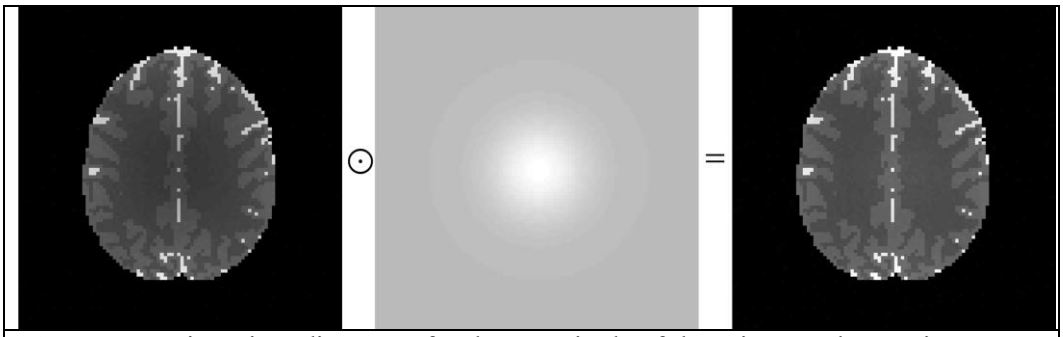

**Figure 11:** Point-wise adjustment for the magnitude of the prior voxel mean image.

The $N_C$ complex-valued averaged calibration images in Figure 10 are pointwise divided by the magnitude of the prior mean in Figure 11 (right) in order to arrive at the prior mean for the real-imaginary coil sensitivities in Figure 12 (top section) with magnitude-phase in Figure 12 (bottom section). The hyper parameter $g_S$ is assessed to be 0.10 to indicate that the uncertainty in the prior sensitivities is ten times larger than that in the observed aliased coil images. The prior mean for the coil sensitivity phase is used for the phase of the prior mean $v_{0P}$.

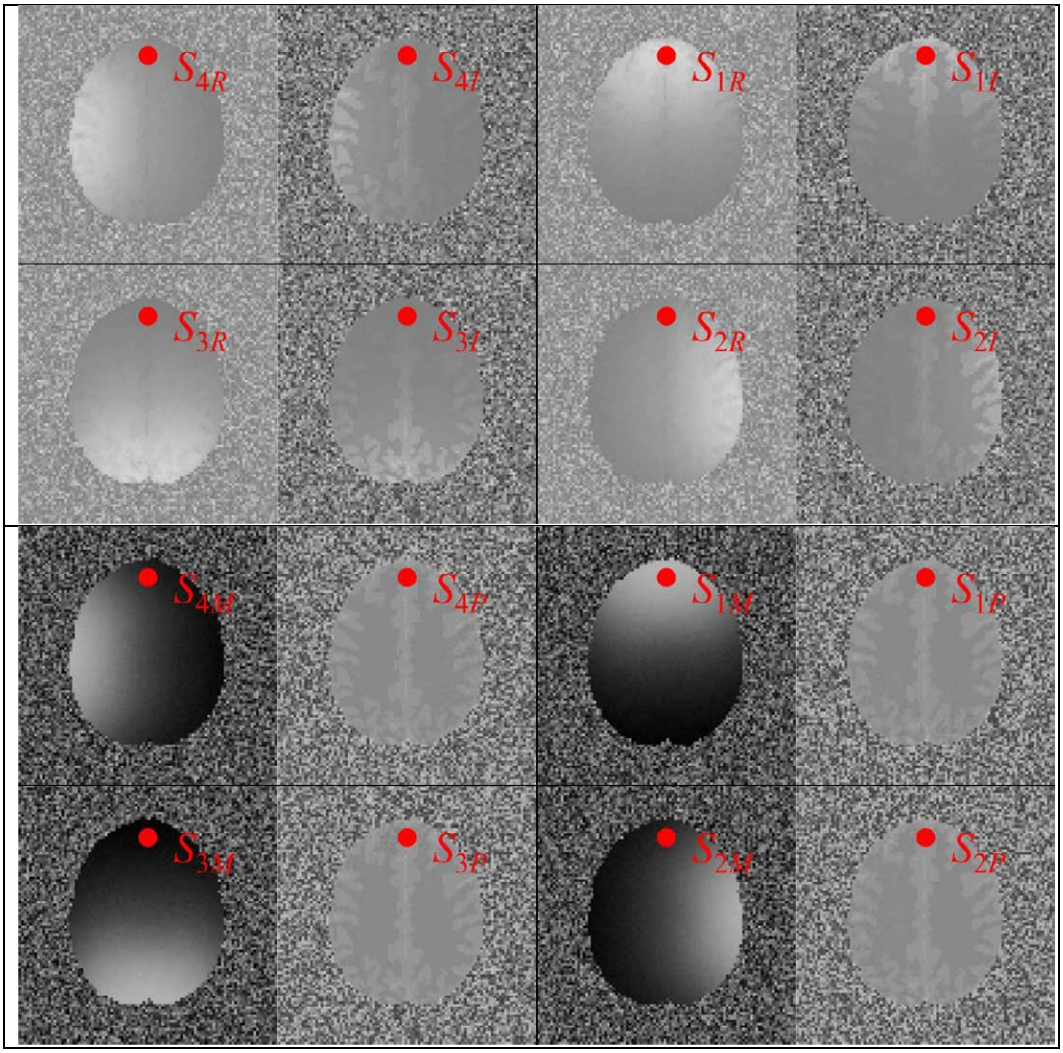

**Figure 12:** Prior mean for coil sensitivities.

The hyper parameters for the residual variance are assessed to be $d$=10 and $q=2d\sigma_0^2$ where $\sigma_0^2$=1.0 is the average residual variance over the voxels of the calibration images.

### 3.2 FMRI Data

To demonstrate the use of BSENSE, a single image was generated for the $N_C$=4 coils by adding $N(0,\sigma^2)$ noise to the noiseless coil images in Figure 9 to arrive at the observed aliased noisy coil images in Figure 13.

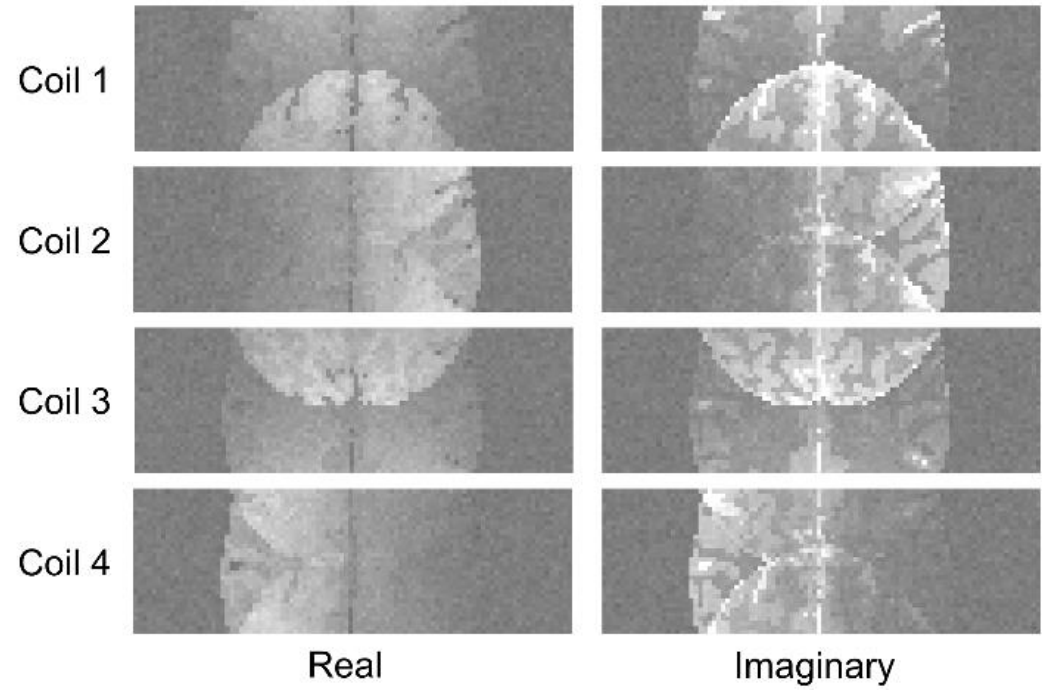


**Figure 13:** Simulated observed noisy coil images for one time point in an fMRI experiment.

### 3.3 Posterior Unaliased Image

Using the previously assessed hyperparameters along with the observed aliased coil images in Figure 13, MAP BSENSE unaliased images are presented in Figure 14.

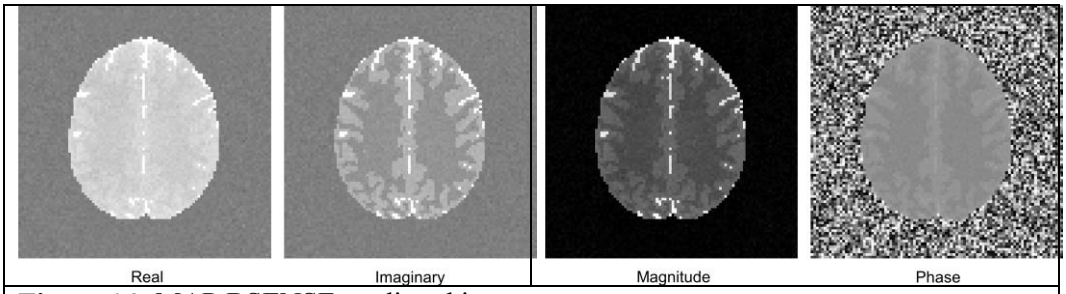


**Figure 14:** MAP BSENSE unaliased images.

We can see that the BSENSE unaliased and combined images with real-imaginary (left) and magnitude-phase (right) appear to be artifact free and a very good estimate of the true noiseless slice images.

## 5. Discussion

A Bayesian model for a latent variable image estimation of the SENSE image combination type was successfully formulated and applied to simulated data. Prior distributions were combined with a likelihood to form a posterior distribution. Hyperparameters were assessed using available calibration images. MAP estimates of the unaliased voxels were computed. This opens up the opportunity for more formal Bayesian models to formally incorporate available prior knowledge to separate accelerated images in fMRI.

## Acknowledgements

This work was supported in part by NIH NS087450.

## References

1. Bandettini P, Jesmanowicz A, Wong E, Hyde J. Processing strategies for time-course data sets in functional MRI of the human brain. Magn Reson Med 30:161–173, 1993.
2. Ogawa S, Lee TM, Nayak AS, Glynn P. Oxygenation-sensitive contrast in magnetic resonance image of rodent brain at high magnetic fields. Magn Reson Med 14(1):68–78, 1990.
3. Kumar A, Welti D, Ernst RR. NMR Fourier zeugmatography. J Magn Reson, 18(1):69–83, 1975.
4. Hyde JS, Jesmanowicz A, Froncisz W, Kneeland JB, Grist TM, Campagna NF. Parallel image acquisition from noninteracting local coils. J Magn Reson, 70:512–517, 1986.
5. Pruessmann KP, Weiger M, Scheidegger MB, Boesiger P. SENSE: Sensitivity Encoding for Fast MRI. Magn Reson Med, 42:952–962, 1999.
6. Griswold MA, Jamob PM, Heidemann RM, Nikkka M, Jellus V, Wang J, Kiefer B, Haase A. Generalized autocalibrating partially parallel acquisition (GRAPPA). Magn Reson Med, 47:1202–1210, 2002.
7. Rowe DB: Image Reconstruction in Functional MRI. In Handbook of Statistical Methods for Brain Signals and Images, Editors Ombao H, Lindquist M, Thompson W, Aston J. Chapman & Hall/CRC Press. p. 205-232, 2016.
8. Rowe DB, Logan BR. A complex way to compute fMRI activation. Neuroimage, 23:1078–1092, 2004.
9. Rowe DB. Modeling both the magnitude and phase of complex-valued fMRI data. Neuroimage, 25(4):1310–1324, 2005.
10. Lindley DV, Smith AFM, Bayes estimates for the linear model, Journal of the Royal Statistical Society B, 34 (1):1–18, 1972.
11. Geman S, Geman, D. Stochastic Relaxation, Gibbs Distributions, and the Bayesian Restoration of Images. IEEE Transactions on Pattern Analysis and Machine Intelligence. 6(6):721–741, 1984.
12. Rowe DB: Multivariate Bayesian Statistics: Models for Source Separation and Signal Unmixing. Chapman & Hall/CRC Press, Boca Raton, FL, 2003.